Dual phase regulation of experimental allergic encephalomyelitis by platelet-activating factor

Yasuyuki Kihara,[1] Satoshi Ishii,[1] Yoshihiro Kita,[1] Akiko Toda,[1] Atsuyoshi Shimada,[2] and Takao Shimizu[1]

[1]Department of Biochemistry and Molecular Biology, Faculty of Medicine, The University of Tokyo, Tokyo 113-0033, Japan
[2]Department of Pathology, Institute for Developmental Research, Aichi Human Service Center, Aichi 480-0392, Japan

Experimental allergic encephalomyelitis (EAE) serves as a model for multiple sclerosis and is considered to be a CD4$^+$ Th1 cell–mediated autoimmune disease. To investigate the role of platelet-activating factor (PAF) in this disease, PAF receptor (PAFR) KO (PAFR-KO) and wild-type (WT) mice, on a C57BL/6 genetic background, were immunized with myelin oligodendrocyte glycoprotein 35–55. The levels of PAF production and PAFR mRNA expression in the spinal cord (SC) correlated with the EAE symptoms. PAFR-KO mice showed lower incidence and less severe symptoms in the chronic phase of EAE than WT mice. However, no difference was observed in T cell proliferation, Th1-cytokine production, or titer of IgG2a between both genotypes. Before onset, as revealed by microarray analysis, mRNAs of inflammatory mediators and their receptors—including IL-6 and CC chemokine receptor 2— were down-regulated in the SC of PAFR-KO mice compared with WT mice. Moreover, in the chronic phase, the severity of inflammation and demyelination in the SC was substantially reduced in PAFR-KO mice. PAFR-KO macrophages reduced phagocytic activity and subsequent production of TNF-α. These results suggest that PAF plays a dual role in EAE pathology in the induction and chronic phases through the T cell–independent pathways.

CORRESPONDENCE
Takao Shimizu:
tshimizu@m.u-tokyo.ac.jp

Abbreviations used: cPLA$_2$, cytosolic phospholipase A$_2$; CNS, central nervous system; EAE, experimental allergic encephalomyelitis; ESI, electrospray ionization; H&E, hematoxylin-eosin; LFB, luxol fast blue; lyso-PAF AT; lyso-PAF acetyltransferase; MCP, monocyte chemoattractant protein; MOG, myelin oligodendrocyte glycoprotein; MS, multiple sclerosis; MS/MS, tandem mass spectrometry; PAF, platelet-activating factor; PAFR, PAF receptor; SC, spinal cord.

Multiple sclerosis (MS) is considered to be a CD4$^+$ T cell–mediated disease that exhibits inflammation and demyelination in the central nervous system (CNS) (1). Although genetic and environmental factors are implicated in the pathogenesis of MS (2), the mechanism for MS remains obscure. Experimental allergic encephalomyelitis (EAE) is an indispensable animal model for a better understanding of MS pathogenesis (3). EAE, as well as MS, seem to be autoimmune diseases because of the presence of CD4$^+$ T cells that are responsive to autoantigens (myelin basic protein, MBP; proteolipid protein, PLP; myelin oligodendrocyte glycoprotein, MOG) and the participation of Th1-type inflammatory molecules (3). Meanwhile, it has been suggested that allergic responses may also play a role in the pathogenesis of EAE (4–6).

Platelet-activating factor (PAF, 1-O-alkyl-2-acetyl-sn-glycero-3-phosphocholine) is a lipid mediator that has biological effects on a variety of cells and organs (7). PAF is produced by various kinds of cells, including neutrophils, eosinophils, monocytes/macrophages, and vascular endothelial cells (8). Bioactivities of PAF are elicited by binding to the PAF receptor (PAFR), which belongs to the superfamily of G protein–coupled seven-transmembrane receptors (9). To elucidate the biological and pathophysiological functions of PAF, we generated PAFR-KO mice and demonstrated that the PAFR deficiency protected mice from many allergic and inflammatory disorders (7, 10–12). Several lines of evidence suggest that PAF may also play a role in autoimmune diseases, like MS/EAE (5, 13, 14). For example, PAF levels were elevated in the cerebrospinal fluid and plasma of patients who had the relapsing-remitting form of MS (13), and increased levels of PAFR transcripts in MS lesions were revealed by gene-microarray analysis (14). PAFR transcripts were also up-regulated in the brain and spinal cord (SC) from SJL mice with EAE (5). Although these studies suggest that PAF contributes to the pathology of MS/EAE through PAFR, much less is known about how PAF affects the pathology of MS or EAE. In the present study,

The online version of this article contains supplemental material.

we induced EAE in PAFR–KO mice and wild-type (PAFR–WT) controls with MOG_{35-55} peptide, and disclosed that PAF worsens EAE pathology in the induction and chronic phases, probably through the T cell–independent pathways.

RESULTS

Changes in PAFR mRNA expression and PAF production in SC were correlated with progression of EAE pathology

To understand the roles of the PAF/PAFR system in EAE pathology, we first examined the levels of PAFR mRNA expression by quantitative real-time PCR and PAF production by reversed-phase HPLC–electrospray ionization (ESI)–tandem mass spectrometry (MS/MS). C57BL/6 mice were immunized with MOG_{35-55} peptide (Fig. 1 A), and SCs were removed from naive mice and EAE mice on days 11, 18, and 30. Expression levels of PAFR transcripts were correlated with the disease progression (Fig. 1 B). Namely, the amounts of PAFR transcripts in almost all SCs of naive mice and EAE mice on day 11 were less than the detection limit. However, PAFR transcripts were elevated dramatically on day 18 and then declined on day 30 to levels that were still higher than those on days 0 and 11. Fig. 1 C shows the PAF levels in SCs of naive and EAE mice. PAF level was 4.3 ± 0.8 pg/mg tissue in naive mice, and tended to increase slightly in EAE mice on day 11 (5.8 ± 0.1 pg/mg tissue). PAF level on day 18 (19.3 ± 0.6 pg/mg tissue) was increased significantly— 4.5 times as much as naive mice (P < 0.001). Meanwhile, PAF level on day 30 (11.3 ± 0.3 pg/mg tissue) was decreased significantly to ∼60% of that on day 18 (P < 0.01), yet remained higher than that in naive mice (P < 0.05). We found a significantly positive correlation between the clinical score and the PAF production in SC (P < 0.0001) (Fig. 1 D). These results suggest that the PAF/PAFR system is essential for the pathogenesis of EAE.

PAFR–KO mice showed less severe symptoms and lower incidence of EAE

PAFR–WT and PAFR–KO mice were immunized with MOG_{35-55} peptide and monitored for up to 42 d. There was a significant difference in the course of the disease between PAFR–WT and PAFR–KO mice (P < 0.0001) (Fig. 2, A and C). Furthermore, the body weight loss in PAFR–WT mice was significantly more severe than that in PAFR–KO mice (P < 0.0001) (Fig. 2, B and D). Clinical parameters of EAE are summarized in Table I. PAFR–KO mice showed a significantly lower incidence of disease (69%) compared with PAFR–WT mice (97%; P < 0.01). The day of disease onset in PAFR–KO mice was similar to that in PAFR–WT mice. The mean maximal score of PAFR–KO mice was significantly lower than that of PAFR–WT mice (P < 0.05); the number of PAFR–KO mice with a maximal score of ≥2.5 was significantly less than that of PAFR–WT mice (P < 0.05).

PAFR deficiency suppressed sustained inflammation in SC

Histological features of EAE are inflammation and demyelination. The lesions were more extensive in SC than in
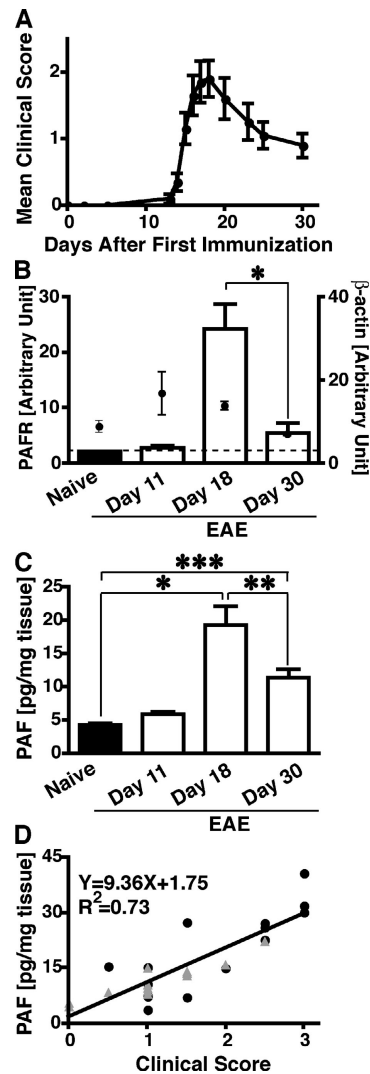

Figure 1. PAFR mRNA expression and PAF production in CNS of MOG_{35-55}–induced EAE mice. (A) C57BL/6 mice were immunized with MOG_{35-55} peptide and monitored for clinical score up to day 30 (n = 10). Data represent means ± SEM. (B) Expression of PAFR mRNA was quantitated by real-time PCR in SC of naive mice and EAE mice on days 11, 18, and 30 (n = 6, 5, 5, and 6, respectively). Bars and circles show the mRNA levels of PAFR and β-actin, respectively. Dotted line represents a detection limit. Data are expressed as means ± SEM. *P < 0.01 by Mann-Whitney U test. (C) PAF level was determined in SC of naive mice and EAE mice on days 11, 18, and 30 (n = 11, 13, 15, and 14, respectively). Data represent means ± SEM. *P < 0.001, **P < 0.01, and ***P < 0.05 by analysis of variance with Tukey-Kramer test. (D) PAF level in SC was correlated positively with the clinical score on days 18 (circle) and 30 (triangle) (Spearman rank correlation test: P < 0.0001, R = 0.85). Each dot represents the result of a single animal.

brain in our model. Thus, SCs from EAE mice were stained with hematoxylin and eosin (H&E) and luxol fast blue (LFB)–cresyl violet to assess the degree of inflammation and demyelination, respectively. Fig. 3 shows representative sections of SC from EAE mice. Severe inflammation was occasionally associated with tissue vacuolation
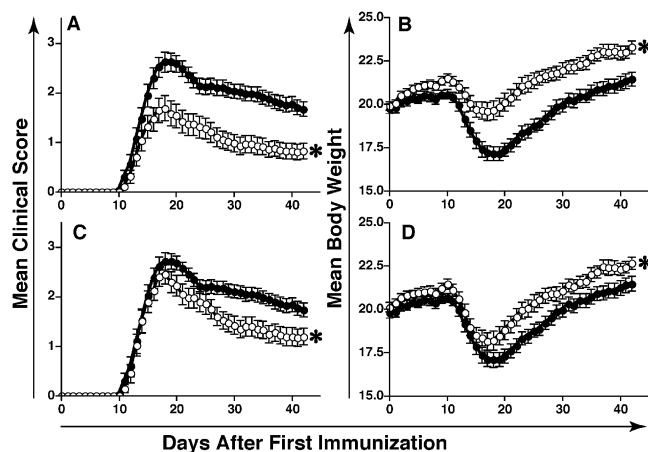
Figure 2. Changes in clinical score and body weight of MOG$_{35-55}$-induced EAE mice. (A and B) PAFR-WT (filled circle) and PAFR-KO (open circle) mice were immunized with MOG$_{35-55}$ peptide and monitored daily for clinical score (A) and body weight (B) up to day 42. Data represent means ± SEM from three independent experiments with a total of 29 animals in each genotype. (C and D) Mean clinical score (C) and mean body weight (D) of only mice with disease onset is shown. Data represent means ± SEM from three independent experiments with a total of 28 and 20 animals for PAFR-WT and PAFR-KO mice, respectively. *P < 0.0001 versus PAFR-WT determined by two-way repeated measures analysis of variance.

(Fig. 3 A), but no vacuolation was observed in naive controls (Fig. 3 B). Inflammatory cells penetrated the pia mater and infiltrated into the perivascular regions and parenchyma; approximately the same number of PMNs was observed in PAFR-WT mice (Fig. 3 C) and PAFR-KO mice (not depicted) in the acute phase of EAE (153 ± 29 and 123 ± 30 PMNs/12 sections of SC, respectively, $n = 4$ animals), but not in the chronic phase of EAE. Because normal myelin of the white matter was highlighted clearly by LFB–cresyl violet staining, myelin pallor (paler areas in the white matter) was identified as demyelinated regions. Although margins of myelin pallor were recognized clearly in the chronic phase of EAE (Fig. 3, F and G), they were obscure in the acute phase (Fig. 3, D and E). Therefore, we did not evaluate the degree of demyelination in the acute phase of the disease. Grading of the sections failed to show a significant difference in the degree of inflammation between PAFR-WT and PAFR-KO mice in the acute phase (Fig. 3 H). Conversely, the degree of inflammation and

Table I. Clinical parameters of MOG$_{35-55}$-induced EAE

Genotype	Incidence	Mean day of onset[a]	Mean maximal clinical score[a]	Number of mice with maximal score ≥2.5
PAFR-WT	28/29	13.6 ± 0.4	2.9 ± 0.2	25
PAFR-KO	20/29[b]	13.1 ± 0.3	2.6 ± 0.2[c]	14[b]

Composite data from three independent experiments are shown.
[a]Mice with score 0 were excluded from the data. Data represent means ± SEM.
[b]P < 0.05 by Fisher's exact test.
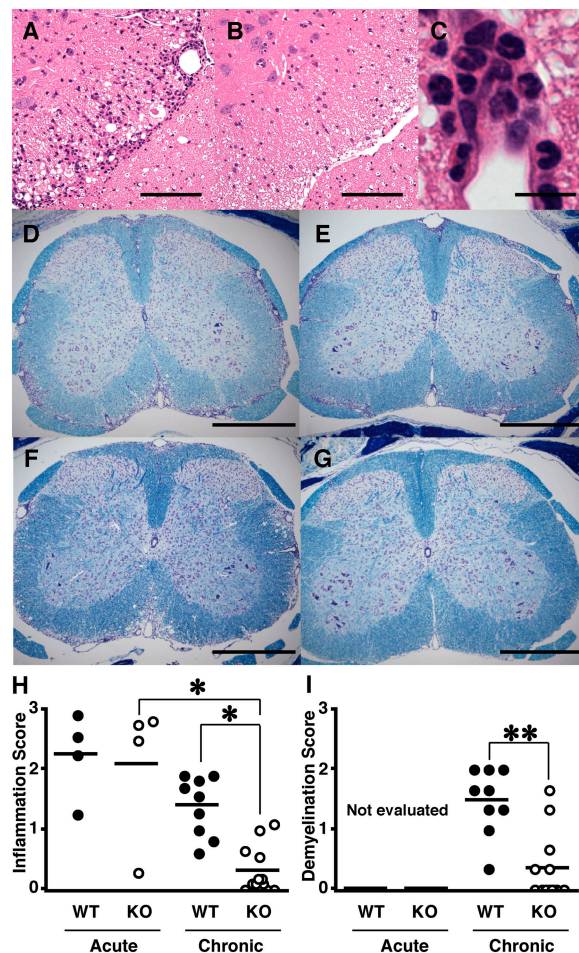[c]P < 0.05 by Mann-Whitney U test, significantly different from the PAFR-WT group.

Figure 3. Histological analysis of SC. (A–C) H&E staining revealed histological features of MOG$_{35-55}$-induced EAE in PAFR-WT mice. Severe inflammation with vacuolation was observed in the anterior and lateral funiculi of SC in EAE mice in the acute phase (day 18) of EAE (A), but not in naive mice (B). Polymorphonuclear cells infiltrated into SC in the acute phase of EAE (C). (D–G) LFB–cresyl violet staining revealed the difference in the severity of demyelination between PAFR-WT (D and F) and PAFR-KO (E and G) mice in the acute (D and E) and chronic (F and G) phases of EAE. Bars, 100 μm (A, B); 10 μm (C); and 500 μm (D–G). (H and I) Histological features were scored semi-quantitatively in the acute ($n = 4$) and chronic ($n = 9$ or 13) phases as described in Materials and methods. The degrees of inflammation (H) and demyelination (I) are shown. Because of unclear borders of the areas of myelin pallor, demyelination was not evaluated in the acute phase. Each dot represents the histological score of a single animal (filled circle, PAFR-WT; open circle, PAFR-KO). The horizontal bars designate the mean values of individual groups. *P < 0.05 by analysis of variance with Dunn's post hoc test. **P < 0.01 by Mann-Whitney U test.

demyelination was significantly lower in PAFR-KO mice than in PAFR-WT mice in the chronic phase of EAE (P < 0.05 and P < 0.01, respectively) (Fig. 3 I).

Next, we performed immunohistochemistry for the microglia/macrophage marker Iba1 (Fig. 4, A and B), because these cells were reported to express a large amount of PAFR (7). In the acute phase of EAE, infiltration of monocytes/macrophages into inflammatory regions in PAFR-

KO mice was equivalent to that in PAFR–WT mice (Fig. 4 C). However, in the chronic phase, monocytes/macrophage infiltration into CNS of PAFR–KO mice was decreased significantly when compared with that of PAFR–WT mice (P < 0.05) (Fig. 4 C).

PAFR–KO mice had normal immune responses against MOG$_{35-55}$ peptide

The immune responses against MOG$_{35-55}$ peptide were investigated to understand the mechanisms underlying the attenuated symptoms of EAE in PAFR–KO mice. Proliferation assays were performed to quantitate the MOG$_{35-55}$-specific proliferative response of T cells generated by immunization with MOG$_{35-55}$ peptide (Fig. 5 A). Among spleen and LN cells on days 11 and 21, PAFR–KO cells had tendencies toward more proliferative responses than did PAFR–WT cells. On day 21, LN cells from PAFR–KO mice were significantly more responsive to MOG$_{35-55}$ peptide than were those from PAFR–WT mice (P < 0.05).

Supernatants from cultured LN and spleen cells on days 11 (not depicted) and 21 (Fig. 5 B) were collected, and production of various cytokines (TNF-α; IFN-γ; IL-2, -4, -5, -6, and -10; monocyte chemoattractant protein (MCP)-1; and IL-12 p70) was determined. Similar production of IFN-γ and TNF-α, well-known Th1-type cytokines, were observed in PAFR–WT and PAFR–KO mice. Intracytoplasmic flow cytometry of MOG$_{35-55}$-treated CD4$^+$ T cells also showed the equivalent production of IFN-γ in PAFR–WT and PAFR–KO mice (2.7 ± 0.3% and 3.2 ± 0.4%, respectively; Fig. 5 C). As for

Th2-type cytokines, IL-4 and -5 production was less than the detection limit in almost all specimens. Equivalent production of IL-6, MCP-1 (Fig. 5 B), and IL-2 and -10 (not depicted) was observed in both genotypes, whereas IL-12 p70 production was less than the detection limit in almost all specimens.

Sera collected on day 42 were analyzed for IgG1 and IgG2a antibodies against the MOG$_{35-55}$ peptide. PAFR–WT and PAFR–KO mice produced similar amounts of IgG2a (Fig. 5 D), a subclass of IgG that is typically associated with a Th1-type phenotype. IgG1 levels were undetectable under the experimental conditions.

Expression of mRNA encoding inflammatory mediators was reduced in SC of PAFR–KO mice, especially just before EAE onset

Gene expression profiles of inflammatory mediators were examined in SCs removed from PAFR–WT and PAFR–KO mice on day 8 (before the onset) and day 21 (after the onset). As shown in Fig. 6 A, about one third of the genes on the membrane were detected before and after onset. The ratios of gene expression between PAFR–WT and PAFR–KO mice before and after onset were calculated to compare the expression profiles (Fig. 6 B). Before the onset, the expression levels of 22 out of 35 detected genes in
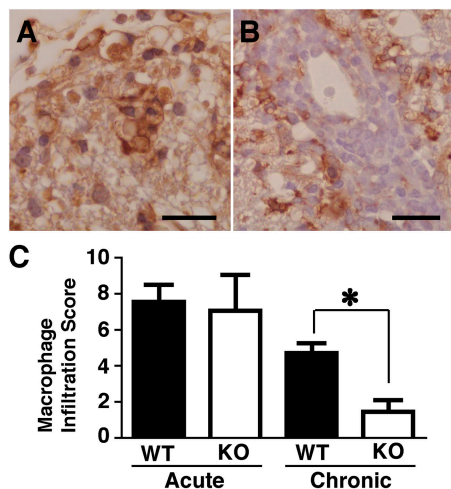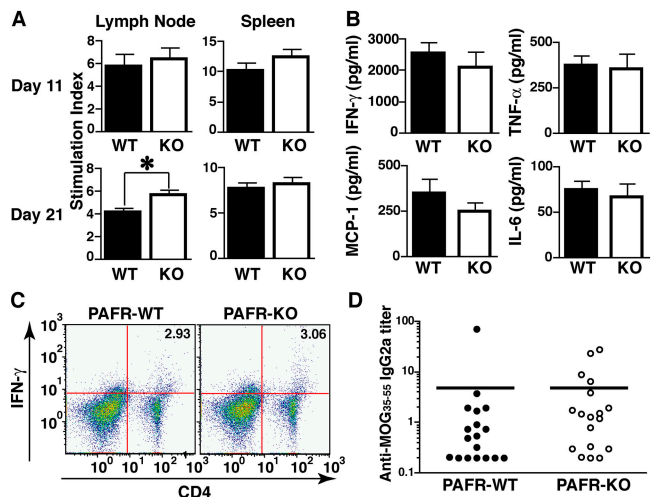

Figure 4. Immunohistochemical staining of microglia/macrophages. (A) Immunohistochemistry revealed intense infiltration of Iba1-positive macrophages just under the pia mater and white matter of SC. (B) Iba1-positive macrophages invaded parenchyma from the perivascular cuffs in the subarachnoidal space. Bars, 20 μm. (C) Monocyte/macrophage infiltration in the inflammatory area was scored as described in Materials and methods (n = 4 animals in the acute phase, n = 9 or 13 animals in the chronic phase). *P < 0.05 by Mann-Whitney U test.

Figure 5. Immune responses against MOG$_{35-55}$ peptide. (A–C) Cells from PAFR–WT (black bar) and PAFR–KO (white bar) mice on days 11 and 21 were stimulated in vitro with MOG$_{35-55}$ peptide. (A) Proliferative responses of LN and spleen cells from EAE mice are shown. *P < 0.05 by Student's t test. (B) Supernatants of LN cell culture on day 21 were used to measure the concentrations of IFN-γ, TNF-α, MCP-1, and IL-6. Data represent means ± SEM from four independent experiments (n = 12 animals). (C) Intracellular staining revealed the population of IFN-γ–producing CD4$^+$ cells. One mouse representative of three mice is shown. (D) Serum was collected 42 d after immunization. Anti-MOG$_{35-55}$ IgG2a titer was assessed by ELISA with a MOG$_{35-55}$ peptide-coated plate. Each dot represents the result of a single animal; the horizontal bars designate the mean values of individual groups. There was no significant difference between PAFR–WT (closed circle) and PAFR–KO (open circle) mice (n = 18 animals).
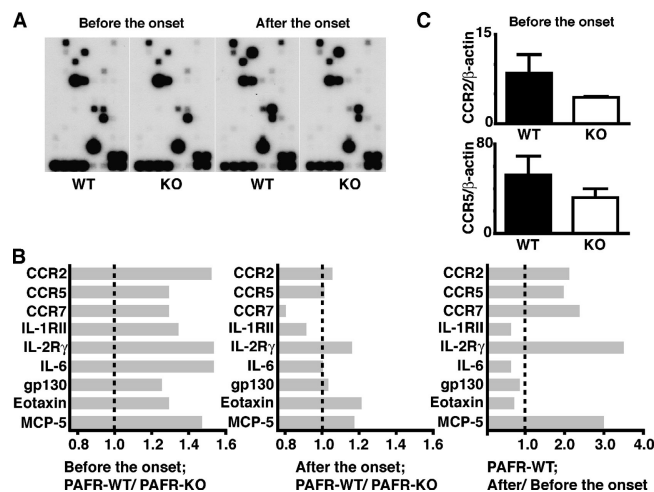
Figure 6. **Effects of PAFR on mRNA expression levels of cytokines, chemokines, and their receptors before and after EAE onset.** (A) Pooled RNA from five SCs of PAFR-WT or PAFR-KO mice was reverse transcribed. The resulting cDNA was hybridized to a membrane printed with cDNA of inflammation-related genes. (B) The ratios of mRNA expression levels in SC of PAFR-WT mice to those of PAFR-KO mice before (left) or after (middle) the onset revealed the changes in expression profiles. The ratios of mRNA expression levels in SC of PAFR-WT "after the onset" to those "before the onset" are also shown (right). Expression levels normalized by β-actin and the ratios of gene expression can be found in Table S1. (C) The higher mRNA expression of CCR2 and CCR5 in PAFR-WT mice over PAFR-KO mice before onset was confirmed by quantitative RT-PCR. Data represent means $\pm$ SEM ($n = 5$ animals).

Figure 7. **Effects of PAF on phagocytic activity of macrophages.** (A) Macrophage phagocytosis of fluorescent particles in the presence or absence of PAF was determined by flow cytometry. Data represent means $\pm$ SEM ($n = 3$). *P $<$ 0.0005 by analysis of variance with Scheffe's test. The results were representative of three independent experiments. (B) TNF-α production upon phagocytosis and the effect of mc-PAF, a nonhydrolyzable agonist of PAFR, were observed. Data represent means $\pm$ SEM ($n = 3$). *P $<$ 0.05 by analysis of variance with Scheffe's test. The results were representative of two independent experiments.

PAFR-WT mice were higher than those in PAFR-KO mice, such as CC chemokine receptor (CCR)2, CCR5, CCR7, IL-1RII, IL-2Rγ, IL-6, gp130, eotaxin, and MCP-5 (Fig. 6 B, left). Higher expression levels of CCR2 and CCR5 in PAFR-WT mice before the onset were confirmed by quantitative RT-PCR (Fig. 6 C; 1.9-fold and 1.6-fold, respectively). After onset, the expression of 16 out of 35 detected genes was more and 15 out of 35 detected genes was less in PAFR-WT mice than in PAFR-KO mice (Fig. 6 B, middle). Fluctuations of the gene expression after the onset seemed to be smaller than those before onset. The differences of gene expression before and after onset in PAFR-WT mice likely reflected the dynamic changes with disease (Fig. 6 B, right), because higher expression of CCR2, CCR5, CCR7, and IL-2Rγ after onset implied that inflammatory cells vigorously infiltrated into CNS with disease development. Similar tendencies were obtained in PAFR-KO mice (Table S1, available at http://www.jem.org/cgi/content/full/jem.20050660/DC1).

PAF affected phagocytic activity in macrophages through PAFR

Demyelination is a result of phagocytosis and subsequent local release of inflammatory mediators by microglia/macrophages. Because of the high expression of PAFR on these cells, phago-
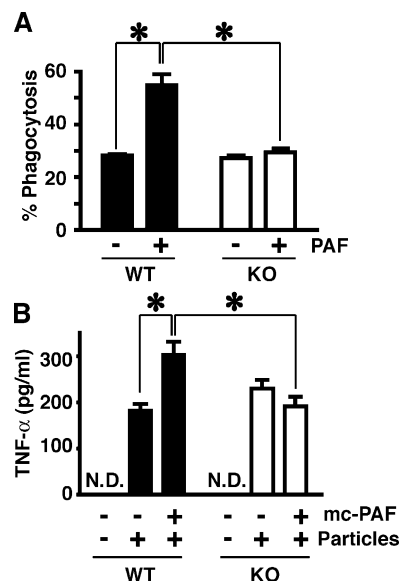
cytic activity of macrophages was measured in the presence or absence of PAF. As shown in Fig. 7 A, the uptake of fluorescent particles was similar between PAFR-WT and PAFR-KO cells in the steady-state. Phagocytosis was enhanced approximately twofold in the presence of PAF in PAFR-WT cells, whereas there was no effect of PAF on PAFR-KO cells. TNF-α production also was up-regulated in association with the enhanced phagocytosis (Fig. 7 B). These results demonstrated that PAF enhanced phagocytosis and TNF-α production through the PAF receptor on macrophages.

DISCUSSION

In this study, we found that PAFR-KO mice, on a C57BL/6 genetic background, showed a lower incidence of MOG$_{35-55}$-induced EAE than did PAFR-WT mice (Table I). In addition, we found that PAFR-KO mice recovered from EAE symptoms significantly faster and more than did PAFR-WT mice (P $<$ 0.0001), although mice of both genotypes showed similar symptoms in the acute phase of the disease (Fig. 2). These results demonstrate the involvement of PAFR in the induction and chronic phases of EAE. Previously, several laboratories studied the effects of PAF antagonists on EAE with conflicting results (5, 15–17). These disparate effects of PAF antagonists may be due to differences in antigens, species, and strains, because the pathology of EAE is known to exhibit large variations depending on these factors. Furthermore, administration of PAF antagonists always

would be accompanied by incomplete inhibition and uncertainty about the specificity of inhibition. However, our present study using PAFR-KO mice clearly showed the important role of PAF in the pathogenesis of MOG$_{35-55}$–induced EAE, at least for mice with a C57BL/6 background.

In many cases of EAE, differences in the severity of the disease can be explained by divergence in the immunological responses to the antigen. Therefore, to address whether the role of PAFR in EAE was associated with alterations in the MOG$_{35-55}$-specific immune responses, we analyzed the proliferative responses and the Th1/Th2 phenotypes of MOG$_{35-55}$-specific T cells from PAFR-KO mice. Proliferation assays showed no impairment in responsiveness of T cells to MOG$_{35-55}$ peptide from PAFR-KO mice (Fig. 5 A). Rather, the proliferative response of PAFR-KO T cells tended to be greater than that of PAFR-WT cells. Because PAF interferes with some processes leading to human CD4$^+$ T cell proliferation (18–20), loss of PAFR signals may enhance T cell proliferation slightly. Th1-type responses, such as production of TNF-α, IFN-γ, and IgG2a, are associated with pathology of EAE (3, 4). Production of these cytokines and autoantibody from PAFR-KO mice were comparable to those from PAFR-WT mice (Fig. 5, B–D). We next measured other cytokine production in vitro to explain the amelioration of the pathology of PAFR-KO mice, because IL-6 (21–27), -10 (28, 29), and -12 (30–32), and MCP-1 (33) were reported to play critical roles in EAE. However, the results did not support a role for PAF in the production of these cytokines (Fig. 5), which suggested that PAFR-WT and PAFR-KO mice were immunized equally by MOG$_{35-55}$ peptide. In addition, PAF was not relevant to Th1-type immune responses during EAE, at least under our experimental conditions. Although allergy and autoimmunity have long been regarded as separate immune responses, Steinman and colleagues (4, 6, 33) proposed that these two pathologies are joined in EAE on the basis of reports of (a) anaphylaxis to self-antigens in EAE mice (34); (b) the ability of Th2–type T cells to induce EAE (35); and (c) the involvement of prostaglandin D synthase, histamine receptor type 1, PAFR, tryptase, and Ig Fcε receptor 1 in EAE (5). Therefore, T cell–dependent and T cell–independent pathways seem to be important for understanding the pathology of EAE. Thus, it is plausible that PAF participates in the pathology of EAE without affecting direct immune responses through Th1-type T cells. Other cells that express PAFR, such as monocytes/macrophages, microglia, PMNs, and endothelial cells, seem to modulate EAE pathology.

It is appropriate for understanding the roles of PAF in EAE to divide the disease course into induction, acute, and chronic phases in accordance with the clinical symptoms (Fig. 8). The day on which the clinical symptoms appear in mice is defined as the onset; the phase before the onset is the induction phase. Accordingly, the day of onset is the boundary between the induction and acute phases. In the induction phase, autoantigen–specific T cells are primed in peripheral lymphoid organs; subsequently, they expand and differentiate

into Th1-type T cells (36). Then, peripherally activated T cells (as well as other inflammatory cells) migrate and invade the CNS (36, 37). Because mice develop clinical symptoms after these events, T cells are associated tightly with regulation of the onset. Various kinds of KO mice that were impaired in Th1-type immune responses showed alterations in the onset (28, 31, 32, 38). The incidence of EAE in PAFR-KO mice was significantly lower than that in PAFR-WT mice (P < 0.05), although the mean day of onset was similar in both genotypes (Table I). Because PAF has little direct effect on the priming, expansion, and differentiation of T cells, PAF may control the onset independently of T cells. If so, how does PAF regulate the onset? Comparison of the mRNA expression profile in SCs of PAFR-WT and PAFR-KO mice seems to account for the regulatory role of PAF in the onset of the disease (Fig. 6 B, left). For example, we observed that IL-6 mRNA expression in SC of PAFR-WT mice was higher than that of PAFR-KO mice before onset (Fig. 6 B, left). IL-6 is notable for the important regulation of the onset of EAE (22, 25). Because spleen and LN cells that were restimulated with MOG$_{35-55}$ peptide in vitro produced comparable amounts of IL-6 in both genotypes (Fig. 5 B), our results suggest that inflammatory cells other than T cells are responsible for the local production of IL-6 in SC in the induction phase. Consistent with a T cell–independent source of IL-6, IL-6$^{-/-}$ mice that were transferred adoptively with encephalitogenic T cells from IL-6$^{+/+}$ mice developed only very mild EAE (22). CCR2 also has been implicated in EAE development through the T cell–independent pathways (39, 40). Fife et al. (39) showed that CCR2$^{-/-}$ mice that were transferred adoptively with MOG$_{35-55}$-specific CCR2$^{+/+}$ T cells failed to develop EAE, and had impaired accumulation of macrophages in CNS. They proposed that CCR2 expression on macrophages was critical for their migration and accumulation into CNS. The down-regulation of CCR2 mRNA in PAFR-KO mice may be due to reduced infiltration of macrophages in CNS in the induction phase of EAE (Fig. 6, B and C). Collectively, in the induction phase of
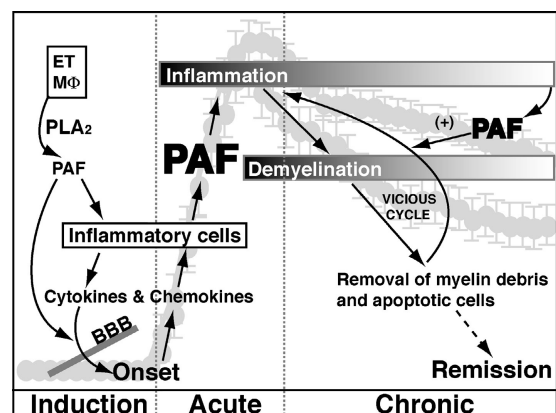

Figure 8. Possible mechanisms of PAF participation in EAE. BBB, blood–brain barrier; ET, endothelial cell; MΦ, macrophage.

EAE, PAF seems to regulate disease onset by modulating cytokine production and accumulation of inflammatory cells in the CNS in a T cell–independent manner.

In the early stage of the acute phase, the clinical course of PAFR-KO mice was equal to that of PAFR-WT mice until the peak of EAE. The relative importance of PAF may be reduced by the severe inflammatory responses that are evoked by various other powerful mediators. Rather, the loss of PAF signaling in inflammatory cells seems to be manifested as time goes on, because PAFR-KO mice showed a significantly lower maximal clinical score than did PAFR-WT mice ($P < 0.05$) (Fig. 2 C; Table I). However, during the peak in the acute phase, the expression profile of inflammation–related genes in PAFR-KO mice was nearly identical to that in PAFR-WT mice (Fig. 6 B, middle). We also observed the histologically equivalent infiltration of inflammatory cells, including PMNs and macrophages that express a large amount of PAFR (7, 41), into SCs in PAFR-WT and PAFR-KO mice (Figs. 3 and 4). The elevated PAF levels at the peak (Fig. 1 C) conceivably worsened the EAE symptoms by affecting PMNs and macrophages without gene induction.

In the chronic phase of EAE, recovery from the disease was faster and more significant in PAFR-KO mice than in PAFR-WT mice ($P < 0.0001$) (Fig. 2). Histologically, milder inflammation and demyelination were observed in PAFR-KO mice (Fig. 3), and the number of microglia/macrophages was reduced in the inflammatory region (Fig. 4). A crucial step in the demyelination process is phagocytosis with subsequent intracellular digestion of myelin by the infiltrated macrophages (42). We showed that PAFR-WT and PAFR-KO macrophages showed similar phagocytic activity without PAF in vitro, whereas addition of PAF enhanced phagocytosis only in PAFR-WT cells (Fig. 7 A). Our results suggest that reduced inflammation and demyelination in PAFR-KO mice are due to the loss of hyperphagocytic activity of microglia/macrophages. As a result of demyelination, myelin debris and apoptotic cells are accumulated in the lesions. Their removal by microglia/macrophages generally serves as repair of the lesions (42–45). Contrary to this notion, it was reported that macrophage phagocytosis of myelin induces the production of inflammatory mediators, such as TNF-α (42), which cause inflammation and oligodendrocyte cell death (46, 47). In fact, TNF-α production from the macrophages upon phagocytosis was enhanced significantly by PAF treatment ($P < 0.05$) (Fig. 7 B). In the chronic phase, PAF may prevent remission and sustain inflammation and demyelination.

Two enzymes are important for the production of PAF by the remodeling pathway (8): (a) cytosolic phospholipase A$_2$ (cPLA$_2$), the main supplier of PAF precursor 1-alkyl-sn-glycero-3-phosphocholine (lyso–PAF) (48); and (b) acetyl CoA:lyso–PAF acetyltransferase (lyso–PAF AT), which catalyzes transacetylation of the acetyl group from acetyl–CoA to lyso–PAF. Kalyvas and David (49) showed that cPLA$_2$α is expressed in CD4$^+$ T cells, endothelial cells early in the course of the disease, and macrophages from mice with se-

vere symptoms. It has been reported that lyso–PAF AT activity is present in macrophages (50) and vascular endothelial cells (51), but not in T cells (52). Because PAFR is expressed highly on endothelial cells and macrophages, PAF activates these cells in an autocrine/paracrine manner and most probably affects the permeability of the blood–brain barrier, accumulation of inflammatory cells in the CNS, and promotion of inflammation (7, 8, 53, 54). Kalyvas and David (49) also showed that blocking of cPLA$_2$ by an arachidonic acid analogue, arachidonyl trifluromethyl ketone, prevented the onset and progression of EAE. Additionally, Marusic et al. (55) showed that cPLA$_2$α$^{-/-}$ mice developed less severe EAE than did cPLA$_2$α$^{+/-}$ mice after adoptive transfer of encephalitogenic cells from cPLA$_2$α$^{+/+}$ mice. WT mice that were transferred adoptively with cPLA$_2$α$^{-/-}$ encephalitogenic cells developed EAE with a delayed onset and lower severity compared with those with cPLA$_2$α$^{+/+}$ cells. These results imply that cPLA$_2$α is critical for regulation of the onset and progression through the T cell–dependent and –independent pathways. Thus, we propose that PAF is a definitive mediator that regulates onset and progression of EAE in a T cell–independent manner tightly associated downstream of cPLA$_2$α. We observed the infiltration of PMNs and monocytes/macrophages into SC in the acute and chronic phases of EAE (Figs. 3 and 4), when the PAF levels were enhanced significantly ($P < 0.001$ and $P < 0.05$, respectively) (Fig. 1 C). Because of their cPLA$_2$α and lyso–PAF AT activities (48, 50), it is likely that these cells are responsible for the T cell–independent PAF production, at least in the acute and chronic phases.

In conclusion, possible PAF functions in EAE are shown in Fig. 8. In the induction phase, PAF may be produced locally in the CNS by endothelial cells and perivascular macrophages. The produced PAF enhances the breakdown of the blood–brain barrier, the migration and accumulation of inflammatory cells in the CNS, and the production of proinflammatory molecules (including IL-6). In the acute phase, the effect of PAF may be masked by the severe inflammatory responses that are elicited by various other powerful mediators. However, in the chronic phase, PAF seems to exacerbate inflammation and demyelination by releasing a variety of cytotoxic mediators from phagocytes, such as TNF-α, leading to a vicious cycle that prevents remission of EAE. Thus, PAF plays a dual role in EAE pathology through the T cell–independent pathways in the induction and chronic phases. Our findings have important implications for the design of new therapies for MS.

MATERIALS AND METHODS

Mice. PAFR-KO mice were produced on a mixed C57BL/6 × 129Ola genetic background as described previously (10). This mutant was backcrossed onto a C57BL/6 genetic background for 10 generations, and then PAFR-WT and PAFR-KO mice, derived from the backcrossed PAFR$^{+/-}$ mice, were independently incrossed for the experiments. Female mice were used at 10–12 wk of age for induction of EAE. The maintenance of the facility and the use of animals were in full compliance with the University of Tokyo's Ethics Committee for Animal Experiments.

Induction and clinical assessment of EAE. MOG$_{35-55}$ (MEVGWYR-SPFSRVVHLYRNGK), corresponding to the fragment of mouse MOG from 35 to 55, was synthesized by QIAGEN. C57BL/6 WT and PAFR-KO mice were immunized s.c. in the flank with 300 μg of MOG$_{35-55}$ peptide in 0.1 ml of PBS and 0.1 ml of CFA containing 0.4 mg of *Mycobacterium tuberculosis* (H37Ra; Difco Laboratories) on days 0 and 7, and were injected i.p. with 250 ng of pertussis toxin (List Biological Laboratories) on days 0 and 2. Mice were weighed daily. The clinical signs of EAE were recorded daily on a scale of 0 to 5 with 0.5 points for intermediate scores. The score was defined as follows; 0, no sign; 0.5, mild loss of tail tone; 1.0, complete loss of tail tone; 1.5, mildly impaired righting reflex; 2.0, abnormal gait and/or impaired righting reflex; 2.5, hind limb paresis; 3.0, hind limb paralysis; 3.5, hind limb paralysis with hind body paresis; 4.0, hind and fore limb paralysis; 4.5, moribund; and 5.0, death. The scoring was performed in a blinded fashion.

Quantification of PAF. SCs of naive mice and EAE mice on days 11, 18, and 30 were removed and frozen immediately with liquid nitrogen until use. The frozen tissues (∼100 mg) were powdered by an SK-100 mill (Tokken Inc.), and lipids were extracted with methanol containing deuterium-labeled 16:0 PAF (Cayman Chemical) as an internal standard. To remove lysophospholipids (mainly lysophosphatidylcholine), which strongly interfered with the detection of PAF by reversed-phase HPLC-ESI-MS/MS, the extracted lipid samples were pretreated as described previously (56) with some modifications. In brief, samples (∼1 ml) were vacuum-evaporated and reconstituted with 50 μl of methanol. Then the solutions were applied to a normal phase HPLC using a silica column (SILICA SG120 S5, 4.6 × 100 mm; Shiseido) at 40°C with an isocratic mobile phase (dichloromethane/methanol/water/formic acid, 63.3:31.7:5:0.01) at a flow rate of 1.0 ml/min. A TSQ Quantum Ultra triple-stage quadrupole mass spectrometer with Ion Max source (Thermo Electron) was used for the online monitoring of the internal standards and lysophosphatidylcholine. The mass spectrometry instrument was operated in negative ESI and selected reaction monitoring mode, whose transitions of 568→59 and 572→59 were used for the specific detection of PAF and deuterium-labeled PAF, respectively, and that of 568→508 was used for the nonselective detection of PAF and 18:0 lysophosphatidylcholine. A splitting tee directed ∼5% of the column effluent to the ESI source, and the predetermined PAF containing fractions were collected. After evaporation and reconstitution with 200 μl of methanol, the samples were quantified by reversed-phase HPLC-ESI-MS/MS as described previously (57, 58).

T cell proliferation, cytokine production, and intracellular cytokine staining. Spleens and LNs (axillary and inguinal) from mice were collected on days 11 and 21 after the first immunization. The organs were dispersed into a single-cell suspension, and the cells were washed and adjusted to 1.5 × 10^6 cells/ml or 0.75 × 10^6 cells/ml in complete RPMI 1640 (containing 10% heat-inactivated FCS, 50 μM 2-mercaptoethanol, 2 mM L-glutamine, 1 mM sodium pyruvate, 5% NCTC-109, and penicillin/streptomycin). Cell suspensions at a volume of 100 μl were added to 96-well plates with or without an equal volume of MOG$_{35-55}$ at a concentration of 50 μg/ml, and incubated for 72 h at 37°C with 5% CO$_2$. For the last 8 h, 25 μl of [³H]thymidine (0.5 μCi; GE Healthcare) was added to each well. The cells were harvested onto UniFilter-GF/C glass filters (PerkinElmer). After the addition of MicroScint-0 scintillation cocktail (PerkinElmer), radioactivities were determined using a TopCount microplate scintillation counter (PerkinElmer). The stimulation index was defined as a ratio of cpm from culture with MOG$_{35-55}$ peptide to that without peptide. For cytokine assays, supernatants were recovered from cell culture plates and stored at −80°C until use. The cytokine assay was performed using the cytometric bead array kit (BD Biosciences). Intracellular staining of cytokines was conducted using Cytofix/Cytoperm kits (BD Biosciences) following the manufacturer's recommendations. FITC-conjugated anti-CD4 antibody (BD Biosciences; clone GK1.5) and PE-conjugated anti–IFN-γ antibody (BD Biosciences; clone XMG1.2) were used as a cell surface marker and for intracellular cytokine staining, respectively. Isotype antibodies were used in parallel as negative controls. The cells were analyzed using an EPIX XL flow cytometer (Beckman Coulter).

Anti–MOG$_{35-55}$ antibody. MOG$_{35-55}$ was dissolved at 1 μg/ml in carbonate buffer (15 mM Na$_2$CO$_3$ and 35 mM NaHCO$_3$, pH 9.5) and was used to coat 96-well plates at 100 μl/well for 3 h at 37°C. The plates were blocked with 2% BSA in PBS for 1 h at room temperature. Sera were obtained from mice 42 d after sensitization. The diluted serum samples (1:20 or 1:40 in 2% BSA/PBS) were added at 100 μl/well and the plates were incubated for 1 h at room temperature and washed three times with 0.05% Tween-20/PBS. After adding horseradish peroxidase-conjugated anti–mouse IgG1 or IgG2a antibody (BD Biosciences) (1:1,000 in 2% BSA/PBS), the plates were incubated for 30 min at room temperature. Substrate solution (3-ethylbenzthiazoline-6-sulfonic acid dissolved in 0.1 M citric acid [pH 4.35]) was added and the absorbance at 405 nm was measured with a plate-reader (Bio-Rad Laboratories).

Histology. On days 18 and 31–32, the mice were anesthetized with urethane and perfused intracardially with 10 ml of ice-cold PBS, followed by 20 ml of 4% paraformaldehyde. SC was fixed overnight in 4% paraformaldehyde. From the paraffin-embedded SC, sections of 5-μm thickness were prepared and stained with H&E or LFB-cresyl violet. 11 or 12 transverse sections from each mouse were observed in a blinded manner to evaluate the degree of inflammation; 3 transverse sections were observed to evaluate demyelination. For evaluation of inflammation, a four-point scale was graded as follows: 0, no sign or minimal inflammation; 1, inflammatory cell infiltrates in meninges; 2, perivascular inflammatory cell infiltrates; and 3, marked infiltration of inflammatory cells into the parenchyma. For evaluation of demyelination, a three-point scale was graded as follows: 0, no sign; 1, crescent-shaped myelin pallor; and 2, semicircular-shaped myelin pallor. The histological score represented the mean of the scores of all sections examined.

Immunohistochemistry. Sections were pretreated with 0.3% solution of H$_2$O$_2$ in methanol containing 0.02% sodium azide to block endogenous peroxidase activity and with 10% normal goat serum in PBS to block nonspecific binding sites, and were incubated at 4°C overnight with a rabbit anti-Iba1 antibody (Wako Pure Chemical Industries), which was diluted 1:250 in PBS containing 10% normal goat serum. Sections were incubated with labeled polymer of the DAKO Envision Plus System (DakoCytomation) at room temperature for 30 min, following the manufacturer's recommendations. The reaction was visualized by incubation with 0.2 mg/ml of 3,3′-diaminobenzidine (Wako Pure Chemical Industries) in 0.05 M Tris-HCl (pH 7.4) containing 3% H$_2$O$_2$ for 5 min. Sections prepared from three levels of the lumbar SC were examined in individual mice. The number of monocytes or macrophages in the area of inflammatory cell infiltrates was graded as one of the four groups according to severity: 0, rare to none; 1, mild; 2, moderate; and 3, marked. The total scores of three sections were compared between PAFR-WT and PAFR-KO mice in each region separately. The scoring was performed in a blinded fashion.

Gene array screening. On days 8 and 21, SCs were removed from EAE mice. Because we could not predict which mice developed EAE before the onset, a pooled sample of total RNA from five mice was used. The mean clinical scores of PAFR-WT and PAFR-KO at day 21 were 2.4 ± 0.5 and 2.0 ± 0.3 ($n = 5$, means ± SEM), respectively. Total RNA was isolated using Absolutely RNA RT-PCR Miniprep Kit (Stratagene). A pooled RNA sample from five EAE mice was reverse-transcribed to cDNA and amplified by linear polymerase replication using the AmpoLabeling-LRP kit (Superarray Bioscience Corp.) with [α-³²P]dCTP (GE Healthcare). The labeled cDNAs were denatured and hybridized overnight because probes to the GEArray membrane focused on mouse inflammatory cytokines and receptors (Superarray Bioscience Corp.). The GEArray images were detected using BAS2000 (Fujifilm), and the radioactivity of each spot was quantified by MacBAS software (Fujifilm). All signals, obtained by subtracting the lowest

measured value from the values of all genes, were normalized to β-actin. The gene expression profile of PAFR-WT mice was compared with that of PAFR-KO mice.

Quantitative real-time PCR. Total RNA was extracted from SC as described before. The purity and integrity of RNA were determined by the absorbance at $A_{260/280}$ and gel electrophoresis, respectively. 1 μg of RNA was reverse-transcribed by using SuperScript II (Invitrogen) according to the manufacturer's instructions. Quantitative PCR for levels of β-actin, CCR2, CCR5, and PAFR mRNA was performed with LightCycler FastStart DNA Master SYBR Green I (Roche). Except for PAFR, Primers were designed across introns to exclude the possibilities of contamination of genomic DNA as follows: CCR2, forward, 5′-CCTGCAAGACCAGAAGAGG-3′, and reverse, 5′-CAAGGCTCACCATCATCGTA-3′; CCR5, forward, 5′-TCCTAGC-CAGAGGAGGTGAG-3′, and reverse, 5′-AGCCGCAATTTGTTTCA-CAT-3′; PAFR, forward, 5′-AGCAGAGTTGGGCTACCAGA-3′, and reverse, 5′-TGCGCATGCTGTAAAACTTC-3′; β-actin, forward, 5′-GCT-GTGCTATGTTGCTCTAGA-3′, and reverse, 5′-AATTGAATGTAGTT-TCATGGATGC-3′. Standard curves for these molecules were generated by performing 1-, 10-, 100-, 1,000- and 10,000-fold dilutions of murine macrophage cDNA samples. The mRNA level for each sample was normalized to β-actin.

Phagocytosis assay. Phagocytosis assays were performed as described previously (59). In brief, primary mouse macrophages were harvested from the peritoneal cavity 3 d after i.p. injection with 2 ml of 4% thioglycollate. Total cell numbers were determined with a hemocytometer after staining with Turk solution (Wako). 5×10^5 cells per well in 24-well plates were cultured in RPMI 1640 supplemented with 10% FACS at 37°C in 5% CO_2. After incubation for 2 h, the medium was removed and washed with assay solution (140 mM NaCl, 5 mM KCl, 2 mM $CaCl_2$, 1 mM $MgCl_2$ and 10 mM Hepes [pH 7.4]). Assay solution with 2 μm fluorescent particles (Polysciences) was added at the ratio of 20 particles/cell with or without 12.5 nM 1-hexadecyl PAF (Cayman Chemical) and incubated for 30 min at 37°C in 5% CO_2. Cells were washed with ice-cold assay solution and gently detached for flow cytometric analysis. For TNF-α detection, the fluorescent particles, with or without 50 nM 1-hexadecyl 2-methylcalbamoyl PAF (mc-PAF; Cayman Chemical), were added to 10^6 cells per well in 24-well plates. After 30 min of incubation at 37°C, cells were washed twice with PBS and 300 μl of culture medium was added. Supernatants were recovered after 24 h and stored at −80°C until use. TNF-α was measured using the cytometric bead array kit (BD Biosciences).

Statistical analysis. Results were expressed as means ± SEM. As appropriate, data were analyzed statistically by means of Student's t test, Mann-Whitney U test, Fisher's exact test, or analysis of variance with Tukey-Kramer, Dunn's, or Scheffe's post hoc test. p-values <0.05 were considered to be statistically significant.

Online supplemental material. Table S1 shows the expression levels of inflammation-related genes in the SC together with the ratios of the gene expression. Online supplemental material is available at http://www.jem.org/cgi/content/full/jem.20050660/DC1.

REFERENCES

1. Steinman, L. 2001. Multiple sclerosis: a two-stage disease. *Nat. Immunol.* 2:762–764.
2. Ermann, J., and C.G. Fathman. 2001. Autoimmune diseases: genes, bugs and failed regulation. *Nat. Immunol.* 2:759–761.
3. Iglesias, A., J. Bauer, T. Litzenburger, A. Schubart, and C. Linington. 2001. T- and B-cell responses to myelin oligodendrocyte glycoprotein in experimental autoimmune encephalomyelitis and multiple sclerosis. *Glia.* 36:220–234.
4. Pedotti, R., J.J. De Voss, L. Steinman, and S.J. Galli. 2003. Involvement of both 'allergic' and 'autoimmune' mechanisms in EAE, MS and other autoimmune diseases. *Trends Immunol.* 24:479–484.
5. Pedotti, R., J.J. DeVoss, S. Youssef, D. Mitchell, J. Wedemeyer, R. Madanat, H. Garren, P. Fontoura, M. Tsai, S.J. Galli, et al. 2003. Multiple elements of the allergic arm of the immune response modulate autoimmune demyelination. *Proc. Natl. Acad. Sci. USA.* 100:1867–1872.
6. Steinman, L. 2003. Optic neuritis, a new variant of experimental encephalomyelitis, a durable model for all seasons, now in its seventieth year. *J. Exp. Med.* 197:1065–1071.
7. Ishii, S., and T. Shimizu. 2000. Platelet-activating factor (PAF) receptor and genetically engineered PAF receptor mutant mice. *Prog. Lipid Res.* 39:41–82.
8. Montrucchio, G., G. Alloatti, and G. Camussi. 2000. Role of platelet-activating factor in cardiovascular pathophysiology. *Physiol. Rev.* 80:1669–1699.
9. Honda, Z., M. Nakamura, I. Miki, M. Minami, T. Watanabe, Y. Seyama, H. Okado, H. Toh, K. Ito, T. Miyamoto, and T. Shimizu. 1991. Cloning by functional expression of platelet-activating factor receptor from guinea-pig lung. *Nature.* 349:342–346.
10. Ishii, S., T. Kuwaki, T. Nagase, K. Maki, F. Tashiro, S. Sunaga, W.H. Cao, K. Kume, Y. Fukuchi, K. Ikuta, et al. 1998. Impaired anaphylactic responses with intact sensitivity to endotoxin in mice lacking a platelet-activating factor receptor. *J. Exp. Med.* 187:1779–1788.
11. Hikiji, H., S. Ishii, H. Shindou, T. Takato, and T. Shimizu. 2004. Absence of platelet-activating factor receptor protects mice from osteoporosis following ovariectomy. *J. Clin. Invest.* 114:85–93.
12. Ishii, S., T. Nagase, H. Shindou, H. Takizawa, Y. Ouchi, and T. Shimizu. 2004. Platelet-activating factor receptor develops airway hyperresponsiveness independently of airway inflammation in a murine asthma model. *J. Immunol.* 172:7095–7102.
13. Callea, L., M. Arese, A. Orlandini, C. Bargnani, A. Priori, and F. Bussolino. 1999. Platelet activating factor is elevated in cerebral spinal fluid and plasma of patients with relapsing-remitting multiple sclerosis. *J. Neuroimmunol.* 94:212–221.
14. Lock, C., G. Hermans, R. Pedotti, A. Brendolan, E. Schadt, H. Garren, A. Langer-Gould, S. Strober, B. Cannella, J. Allard, et al. 2002. Gene-microarray analysis of multiple sclerosis lesions yields new targets validated in autoimmune encephalomyelitis. *Nat. Med.* 8:500–508.
15. Howat, D.W., N. Chand, P. Braquet, and D.A. Willoughby. 1989. An investigation into the possible involvement of platelet activating factor in experimental allergic encephalomyelitis in rats. *Agents Actions.* 27:473–476.
16. Desai, S., and R. Barton. 1990. Role of platelet activating factor in the pathogenesis of active and passive models of experimental allergic encephalomyelitis in the rat. *Agents Actions.* 31:43–46.
17. Vela, L., A. Garcia Merino, S. Fernandez-Gallardo, M. Sanchez Crespo, J.J. Lopez Lozano, and C. Saus. 1991. Platelet-activating factor antagonists do not protect against the development of experimental autoimmune encephalomyelitis. *J. Neuroimmunol.* 33:81–86.
18. Dulioust, A., E. Vivier, P. Salem, J. Benveniste, and Y. Thomas. 1988. Immunoregulatory functions of paf-acether. I. Effect of paf-acether on CD4+ cell proliferation. *J. Immunol.* 140:240–245.
19. Rola-Pleszczynski, M., C. Pouliot, S. Turcotte, B. Pignol, P. Braquet, and L. Bouvrette. 1988. Immune regulation by platelet-activating factor. I. Induction of suppressor cell activity in human monocytes and

CD8+ T cells and of helper cell activity in CD4+ T cells. *J. Immunol.* 140:3547–3552.

20. Dulioust, A., V. Duprez, C. Pitton, P. Salem, A. Hemar, J. Benveniste, and Y. Thomas. 1990. Immunoregulatory functions of paf-acether. III. Down-regulation of CD4+ T cells high-affinity IL-2 receptor expression. *J. Immunol.* 144:3123–3129.

21. Eugster, H.P., K. Frei, M. Kopf, H. Lassmann, and A. Fontana. 1998. IL-6-deficient mice resist myelin oligodendrocyte glycoprotein-induced autoimmune encephalomyelitis. *Eur. J. Immunol.* 28:2178–2187.

22. Mendel, I., A. Katz, N. Kozak, A. Ben-Nun, and M. Revel. 1998. Interleukin-6 functions in autoimmune encephalomyelitis: a study in gene-targeted mice. *Eur. J. Immunol.* 28:1727–1737.

23. Okuda, Y., S. Sakoda, C.C. Bernard, H. Fujimura, Y. Saeki, T. Kishimoto, and T. Yanagihara. 1998. IL-6-deficient mice are resistant to the induction of experimental autoimmune encephalomyelitis provoked by myelin oligodendrocyte glycoprotein. *Int. Immunol.* 10:703–708.

24. Samoilova, E.B., J.L. Horton, B. Hilliard, T.S. Liu, and Y. Chen. 1998. IL-6-deficient mice are resistant to experimental autoimmune encephalomyelitis: roles of IL-6 in the activation and differentiation of autoreactive T cells. *J. Immunol.* 161:6480–6486.

25. Okuda, Y., S. Sakoda, H. Fujimura, Y. Saeki, T. Kishimoto, and T. Yanagihara. 1999. IL-6 plays a crucial role in the induction phase of myelin oligodendrocyte glucoprotein 35-55 induced experimental autoimmune encephalomyelitis. *J. Neuroimmunol.* 101:188–196.

26. Okuda, Y., S. Sakoda, Y. Saeki, T. Kishimoto, and T. Yanagihara. 2000. Enhancement of Th2 response in IL-6-deficient mice immunized with myelin oligodendrocyte glycoprotein. *J. Neuroimmunol.* 105:120–123.

27. Eugster, H.P., K. Frei, F. Winkler, U. Koedel, W. Pfister, H. Lassmann, and A. Fontana. 2001. Superantigen overcomes resistance of IL-6-deficient mice towards MOG-induced EAE by a TNFR1 controlled pathway. *Eur. J. Immunol.* 31:2302–2312.

28. Cua, D.J., B. Hutchins, D.M. LaFace, S.A. Stohlman, and R.L. Coffman. 2001. Central nervous system expression of IL-10 inhibits autoimmune encephalomyelitis. *J. Immunol.* 166:602–608.

29. Fillatreau, S., C.H. Sweenie, M.J. McGeachy, D. Gray, and S.M. Anderton. 2002. B cells regulate autoimmunity by provision of IL-10. *Nat. Immunol.* 3:944–950.

30. Gran, B., G.X. Zhang, S. Yu, J. Li, X.H. Chen, E.S. Ventura, M. Kamoun, and A. Rostami. 2002. IL-12p35-deficient mice are susceptible to experimental autoimmune encephalomyelitis: evidence for redundancy in the IL-12 system in the induction of central nervous system autoimmune demyelination. *J. Immunol.* 169:7104–7110.

31. Zhang, G.X., B. Gran, S. Yu, J. Li, I. Siglienti, X. Chen, M. Kamoun, and A. Rostami. 2003. Induction of experimental autoimmune encephalomyelitis in IL-12 receptor–beta 2-deficient mice: IL-12 responsiveness is not required in the pathogenesis of inflammatory demyelination in the central nervous system. *J. Immunol.* 170:2153–2160.

32. Zhang, G.X., S. Yu, B. Gran, J. Li, I. Siglienti, X. Chen, D. Calida, E. Ventura, M. Kamoun, and A. Rostami. 2003. Role of IL-12 receptor beta 1 in regulation of T cell response by APC in experimental autoimmune encephalomyelitis. *J. Immunol.* 171:4485–4492.

33. Huang, D.R., J. Wang, P. Kivisakk, B.J. Rollins, and R.M. Ransohoff. 2001. Absence of monocyte chemoattractant protein 1 in mice leads to decreased local macrophage recruitment and antigen-specific T helper cell type 1 immune response in experimental autoimmune encephalomyelitis. *J. Exp. Med.* 193:713–726.

34. Pedotti, R., D. Mitchell, J. Wedemeyer, M. Karpuj, D. Chabas, E.M. Hattab, M. Tsai, S.J. Galli, and L. Steinman. 2001. An unexpected version of horror autotoxicus: anaphylactic shock to a self-peptide. *Nat. Immunol.* 2:216–222.

35. Lafaille, J.J., F.V. Keere, A.L. Hsu, J.L. Baron, W. Haas, C.S. Raine, and S. Tonegawa. 1997. Myelin basic protein-specific T helper 2 (Th2) cells cause experimental autoimmune encephalomyelitis in immunodeficient hosts rather than protect them from the disease. *J. Exp. Med.* 186:307–312.

36. Miller, S.D., and E.M. Shevach. 1998. Immunoregulation of experimental autoimmune encephalomyelitis: editorial overview. *Res. Immunol.* 149:753–759.

37. Ransohoff, R.M., P. Kivisakk, and G. Kidd. 2003. Three or more routes for leukocyte migration into the central nervous system. *Nat. Rev. Immunol.* 3:569–581.

38. Teuscher, C., M.E. Poynter, H. Offner, A. Zamora, T. Watanabe, P.D. Fillmore, J.F. Zachary, and E.P. Blankenhorn. 2004. Attenuation of Th1 effector cell responses and susceptibility to experimental allergic encephalomyelitis in histamine H2 receptor knockout mice is due to dysregulation of cytokine production by antigen-presenting cells. *Am. J. Pathol.* 164:883–892.

39. Fife, B.T., G.B. Huffnagle, W.A. Kuziel, and W.J. Karpus. 2000. CC chemokine receptor 2 is critical for induction of experimental autoimmune encephalomyelitis. *J. Exp. Med.* 192:899–905.

40. Izikson, L., R.S. Klein, I.F. Charo, H.L. Weiner, and A.D. Luster. 2000. Resistance to experimental autoimmune encephalomyelitis in mice lacking the CC chemokine receptor (CCR)2. *J. Exp. Med.* 192: 1075–1080.

41. Chao, W., and M.S. Olson. 1993. Platelet-activating factor: receptors and signal transduction. *Biochem. J.* 292:617–629.

42. van der Laan, L.J., S.R. Ruuls, K.S. Weber, I.J. Lodder, E.A. Dopp, and C.D. Dijkstra. 1996. Macrophage phagocytosis of myelin in vitro determined by flow cytometry: phagocytosis is mediated by CR3 and induces production of tumor necrosis factor-alpha and nitric oxide. *J. Neuroimmunol.* 70:145–152.

43. Stoll, G., and S. Jander. 1999. The role of microglia and macrophages in the pathophysiology of the CNS. *Prog. Neurobiol.* 58:233–247.

44. Slobodov, U., F. Reichert, R. Mirski, and S. Rotshenker. 2001. Distinct inflammatory stimuli induce different patterns of myelin phagocytosis and degradation in recruited macrophages. *Exp. Neurol.* 167:401–409.

45. Smith, M.E. 2001. Phagocytic properties of microglia in vitro: implications for a role in multiple sclerosis and EAE. *Microsc. Res. Tech.* 54: 81–94.

46. Buntinx, M., M. Moreels, F. Vandenabeele, I. Lambrichts, J. Raus, P. Steels, P. Stinissen, and M. Ameloot. 2004. Cytokine-induced cell death in human oligodendroglial cell lines: I. Synergistic effects of IFN-gamma and TNF-alpha on apoptosis. *J. Neurosci. Res.* 76:834–845.

47. Buntinx, M., E. Gielen, P. Van Hummelen, J. Raus, M. Ameloot, P. Steels, and P. Stinissen. 2004. Cytokine-induced cell death in human oligodendroglial cell lines. II: Alterations in gene expression induced by interferon–gamma and tumor necrosis factor-alpha. *J. Neurosci. Res.* 76:846–861.

48. Shindou, H., S. Ishii, N. Uozumi, and T. Shimizu. 2000. Roles of cytosolic phospholipase A(2) and platelet-activating factor receptor in the Ca-induced biosynthesis of PAF. *Biochem. Biophys. Res. Commun.* 271: 812–817.

49. Kalyvas, A., and S. David. 2004. Cytosolic phospholipase A2 plays a key role in the pathogenesis of multiple sclerosis-like disease. *Neuron.* 41:323–335.

50. Shindou, H., S. Ishii, M. Yamamoto, K. Takeda, S. Akira, and T. Shimizu. 2005. Priming effect of lipopolysaccharide on acetyl-coenzyme A:lyso-platelet-activating factor acetyltransferase is MyD88 and TRIF independent. *J. Immunol.* 175:1177–1183.

51. Holland, M.R., M.E. Venable, R.E. Whatley, G.A. Zimmerman, T.M. McIntyre, and S.M. Prescott. 1992. Activation of the acetyl-coenzyme A:lysoplatelet-activating factor acetyltransferase regulates platelet-activating factor synthesis in human endothelial cells. *J. Biol. Chem.* 267:22883–22890.

52. Garcia, M.C., C. Garcia, M.A. Gijon, S. Fernandez-Gallardo, F. Mollinedo, and M. Sanchez Crespo. 1991. Metabolism of platelet-activating factor in human haematopoietic cell lines. Differences between myeloid and lymphoid cells. *Biochem. J.* 273:573–578.

53. Kumar, R., S.A. Harvey, M. Kester, D.J. Hanahan, and M.S. Olson. 1988. Production and effects of platelet-activating factor in the rat brain. *Biochim. Biophys. Acta.* 963:375–383.

54. Park, T.S., E.R. Gonzales, and J.M. Gidday. 1999. Platelet-activating factor mediates ischemia-induced leukocyte-endothelial adherence in newborn pig brain. *J. Cereb. Blood Flow Metab.* 19:417–424.

55. Marusic, S., M.W. Leach, J.W. Pelker, M.L. Azoitei, N. Uozumi, J.

Cui, M.W.H. Shen, C.M. DeClercq, J.S. Miyashiro, B.A. Carito, et al. Cytosolic phospholipase A2α-deficient mice are resistant to experimental autoimmune encephalomyelitis. *J. Exp. Med.* 202:841–851.

56. Owen, J.S., R.L. Wykle, M.P. Samuel, and M.J. Thomas. 2005. An improved assay for platelet-activating factor using HPLC-tandem mass spectrometry. *J. Lipid Res.* 46:373–382.

57. Kita, Y., T. Takahashi, N. Uozumi, and T. Shimizu. 2005. A multiplex quantitation method for eicosanoids and platelet-activating factor using column-switching reversed-phase liquid chromatography-tan-dem mass spectrometry. *Anal. Biochem.* 342:134–143.

58. Kita, Y., T. Takahashi, N. Uozumi, L. Nallan, M.H. Gelb, and T. Shimizu. 2005. Pathway-oriented profiling of lipid mediators in macrophages. *Biochem. Biophys. Res. Commun.* 330:898–906.

59. Ichinose, M., N. Hara, M. Sawada, and T. Maeno. 1994. A flow cytometric assay reveals an enhancement of phagocytosis by platelet activating factor in murine peritoneal macrophages. *Cell. Immunol.* 156:508–518.